# Sperm-Hybrid Micromotor for Targeted Drug Delivery

Haifeng Xu,[†] Mariana Medina-Sánchez,[*,†] Veronika Magdanz,[†] Lukas Schwarz,[†] Franziska Hebenstreit,[†] and Oliver G. Schmidt[†,‡]

[†]Institute for Integrative Nanosciences, IFW Dresden, Helmholtzstraße 20, 01069 Dresden, Germany
[‡]Material Systems for Nanoelectronics, Chemnitz University of Technology, Reichenhainer Straße 70, 09107 Chemnitz, Germany

Ⓢ *Supporting Information*

**ABSTRACT:** A sperm-driven micromotor is presented as a targeted drug delivery system, which is appealing to potentially treat diseases in the female reproductive tract. This system is demonstrated to be an efficient drug delivery vehicle by first loading a motile sperm cell with an anticancer drug (doxorubicin hydrochloride), guiding it magnetically, to an *in vitro* cultured tumor spheroid, and finally freeing the sperm cell to deliver the drug locally. The sperm release mechanism is designed to liberate the sperm when the biohybrid micromotor hits the tumor walls, allowing it to swim into the tumor and deliver the drug through the sperm−cancer cell membrane fusion. In our experiments, the sperm cells exhibited a high drug encapsulation capability and drug carrying stability, conveniently minimizing toxic side effects and unwanted drug accumulation in healthy tissues. Overall, sperm cells are excellent candidates to operate in physiological environments, as they neither express pathogenic proteins nor proliferate to form undesirable colonies, unlike other cells or microorganisms. This sperm-hybrid micromotor is a biocompatible platform with potential application in gynecological healthcare, treating or detecting cancer or other diseases in the female reproductive system.

**KEYWORDS:** *sperm, biohybrid micromotor, tumor targeting, drug delivery, gynecologic cancers, in situ mechanical release*
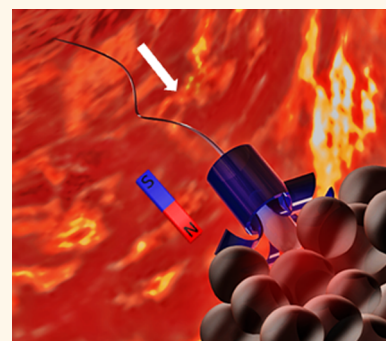
The development of drug delivery systems that provide effective doses locally in a controlled way is one of the main goals in the worldwide fight against cancer.[1,2] The current challenges include the unspecific uptake by other organs,[3] limited tissue penetration,[4] and the decrease of effective concentration due to the dilution in body fluids.[5] Among the most promising nano- and microcarrier approaches to overcome such hurdles are cellular drug delivery systems, where cells or microorganisms act as drug carriers, as they have advantages like membrane fluidity, ability to interact with other cells/tissue, long lifespan, and high biocompatibility.[6] Stem cells, for example, have been used as a combinatorial drug delivery system toward regenerative therapy.[7] Macrophages and red blood cells with and without synthetic guidance or propulsion components have been reported as carriers for cancer therapy[8] and sustained drug release in blood,[9] respectively. Likewise, self-propelled cells, as a combination of cellular encapsulation and propulsion, have interested scientists all over the world due to their swimming performance in complex physiological microenvironments.[10,11] Bacteria, with chemotactic properties[13] and/or with associated synthetic guidance components,[14−16] were shown to actively transport and deliver drugs into tumor tissue. For example, magneto-aerotactic bacteria were reported to deliver drug-loaded

liposomes to the hypoxic regions of tumor tissue in mice.[12] Nonetheless, it is noteworthy that rapid clearance or even autoimmune reactions might be caused by the immune response to certain bacteria.[17]

Compared to other cellular drug carriers, sperms are naturally optimized to swim in the female reproductive system, which makes them promising candidates for the treatment of cervical cancer and other gynecologic diseases. Sperm cells also have the extraordinary ability to encapsulate hydrophilic drugs, which have high DNA-binding affinity,[18] storing them in its crystalline nucleus.[19] By doing so, the sperm membrane can protect drugs from body fluid dilution, immune reactions, and the degradation by enzymes. Sperms can also efficiently avoid dose dumping, which is regarded as a major issue of micelle carriers, thanks to their compact membrane system.[20] To achieve targeted drug delivery, some fruitful attempts have also been shown by using synthetic micromotors. For example, artificial flagellae have been reported for gene transfection of human embryonic kidney HEK 293 cells, through the transport of pDNA-loaded lipoplexes[21] and for the cargo-release of
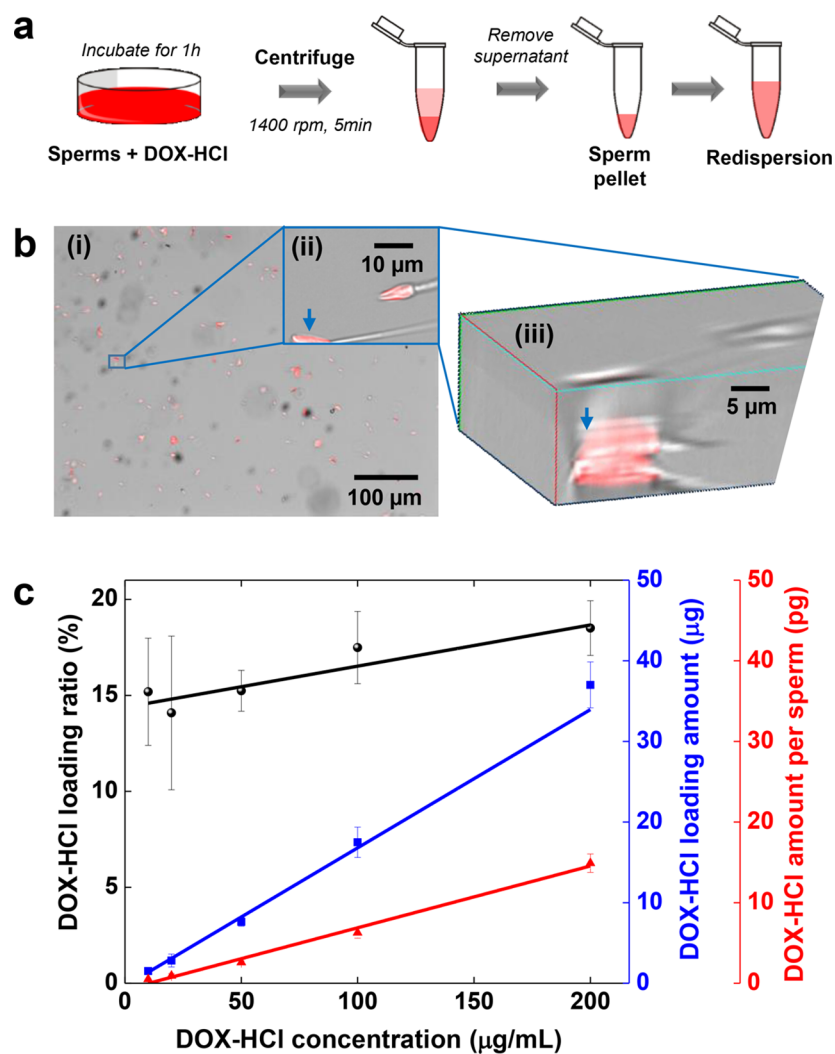
Figure 1. (a) Experimental flowchart for loading DOX-HCl into sperms. (b) Fluorescence and bright-field overlay images of DOX-HCl-loaded sperms in (i) 10× and (ii) 40×, (iii) 3D reconstruction of 36 z-stack images with stack separation distance of 0.3 μm. (c) Plots of the drug loading results *versus* DOX-HCl concentrations in the loading solution (error bars represent the standard deviation of 4 replicates). The drug loading ratio is obtained by the ratio of the encapsulated DOX-HCl into the sperms by the original amount of DOX-HCl in solution. The drug loading amount is the encapsulated amount of DOX-HCl in 500 μL of sperm solution at a concentration of $3 \times 10^6$ sperms/mL. The drug loading efficiency was evaluated by calculating the loading ratio, *i.e.*, the ratio of the amount of drug loaded into sperms to the initial drug amount in solution.

calcein-loaded liposomes to single mouse myoblasts *in vitro*.[22] Mg-based micromotors were also successfully used to deliver drugs in a mouse stomach to treat bacterial infections.[23] However, considering the application of cancer treatment in the female reproductive tract, sperms are more suitable candidates to transport drugs than purely synthetic micromotors as they are naturally adapted to swim in such environment and possess practical advantages such as payload protection and reduced cytotoxicity thanks to their compact membrane. Moreover, for synthetic microcarriers such as microspheres, microcapsules, and drug-loaded micromotors,[24−26] the drug transfer is a problematic issue due to the inefficient transmembrane transport between the carriers and the unhealthy cells.[27] In contrast, sperm cells, with their somatic cell-fusion ability are expected to improve the drug transfer to the target cells, as well as the drug availability. Several proteins of the sperm membrane such as CD9 and integrins are involved in this process.[28] Previous studies demonstrated the use of sperms as carriers of nanoparticles[29] and lipid vesicles[30] on their membrane for

protein localization and biomacromolecule transport, respectively. In addition, micromotors have been employed to carry or guide sperm cells toward assisted *in vivo* fertilization.[10,31,32] However, to our knowledge, no existing application of sperms for drug delivery has been reported before. Thus, we present a sperm-hybrid micromotor for targeted drug delivery. This system comprises a motile sperm cell that serves as the propulsion source and drug carrier and a 3D-printed magnetic tubular microstructure (termed "tetrapod") that features four arms which release the sperm cell *in situ* when they are bent upon pushing against a tumor spheroid. Providing controllable guiding and release mechanisms, this micromotor can potentially deliver drugs to tumor cells and furthermore avoid undesired drug accumulation in healthy tissue. This system combines several intriguing features, namely, high drug loading capacity, self-propulsion, *in situ* mechanical trigger release of the drug-loaded sperm, sperm penetration ability, and improved drug availability.

## RESULTS AND DISCUSSION

**Drug Loading into Sperms.** Figure 1 illustrates the drug loading into sperm cells. Doxorubicin hydrochloride (DOX-HCl) was used as a model drug to evaluate the encapsulation performance of sperm cells. It is a widely approved chemotherapeutic medication with a broad application spectrum in cancer therapy since 1974.[33] Its liposomal form (Doxil) is also used primarily for gynecologic cancer treatment.[34] In this research, DOX-HCl-loaded sperms were obtained by simple co-incubation of DOX-HCl and bovine sperms (see details in the Methods section). After purification, the incubated sperm sample was redispersed in the sperm medium (SP-TALP) (Figure 1a). The drug loading of sperms was evaluated by fluorescence microscopy, as shown in Figure 1b(i), as DOX-HCl exhibits self-fluorescence at 470 nm excitation wavelength. From these images, it was calculated that 98% of the sperm cells (ca. 3500 sperm cells) were loaded with DOX-HCl. DOX-HCl was predominately found in the head of sperms, as can be observed in Figure 1b(ii). A detailed 3D reconstructed image, obtained from overlaid z-stack images of a single sperm cell, indicates that DOX-HCl was mainly loaded into the cytoplasm and the nucleus of the sperm (Figure 1b(iii)). This can be attributed to the drug adsorption on the condensed chromosomes by binding to proteasomes[35] and the drug dispersion in the cytoplasm that remains in the head of the sperm after maturation.[29,36] As a complementary experiment, we loaded sperms with fluorescein isothiocyanate labeled bovine serum albumin (FITC-BSA), a model for protein drugs as an alternative control. In this case, sperms accumulated drug in their heads, midpieces, and tails, which can be attributed to their ability to absorb proteins (Figure S1). Further studies using protein-based drugs must be done in order to evaluate their biodistribution and therapeutic effect in order to draw a conclusive comparison to DOX-HCl, which was chosen for further experiments in this study.

Figure 1c depicts the drug loading profiles related to DOX-HCl concentration. In the solution with a concentration of $3 \times 10^6$ sperms per mL, the loading amount of DOX-HCl increased approximatively linearly with the concentration of DOX-HCl ranging from 10 to 200 $\mu$g/mL. Hence, the loading ratio remains at around 15% for all concentrations. For the maximum concentration of DOX-HCl in our experiments, the loading amount was up to 37 $\mu$g in 500 $\mu$L of sperm solution. This amount indicates an average encapsulation of 15 pg of DOX-HCl per single sperm cell.

The result of the drug loading ratio calculation highlights the high encapsulation capacity of sperm cells. Previous research showed successful loading of DOX into macrophages,[37] where DOX was found inside the cells (2.5 pg per cell), particularly in the nucleus, with a higher concentration compared to the residual DOX solution in the culture medium (cell size roughly 15−20 $\mu$m). To explain this loading profile, the authors referred to the adenosine triphosphate (ATP)-mediated permeabilization of cells as a possible encapsulation mechanism.[37] In our research, DOX-HCl was used because cells also exhibit improved uptake of ionic DOX-HCl[38] compared to molecular DOX, which is normally uptaken by facilitated diffusion.[33] This could allow the use of high local doses of anticancer drugs while reducing systemic toxic effects. Further research is required to investigate in detail the drug transport mechanism through the sperm membrane.

In order to analyze the influence of DOX-HCl on sperms, two complementary tests were performed. First, the viability of DOX-HCl-loaded sperms was analyzed using a commercial LIVE/DEAD kit (Figure S2). No significant difference was observed compared to unloaded sperms as more than 30% of sperms were still alive in both cases after 4 h of culture in SP-TALP. As a more direct study to determine the most apt sperms for the intended goal of drug delivery, a sperm motility test was suggested, as it not only provides information about the sperm's viability but also about their ability to transport the drug. Figure S3 shows the motility change of sperms after the loading process of DOX-HCl at 100 $\mu$g/mL. A control sample with unloaded sperms was incubated in SP-TALP without drug under the same incubation and purification conditions. Motilities of both sperm samples decreased over time similarly. In the first 4 h, the percentage of motile sperms decreased from ca. 56 to 36%, which is sufficient to couple to the microscaffolds for the subsequent experiments. After 8 h of incubation, ca. 25% of sperms were still motile in both groups. Thus, we suggest to perform the drug delivery experiment within 8 h after the drug-loading step, which is sufficient to reach any organ from the reproductive system (the maximum traveling distance in our experiments was about 144 cm, considering an average velocity of the sperm-hybrid micromotor of 50 $\mu$m/s). Thus, the influence of DOX-HCl on sperm viability is not significant. This can be explained by the fact that DOX-HCl kills cancer cells by interfering with their macromolecular biosynthesis.[39] Unlike cancer cells, mature sperms have terminated most of their macromolecular synthesis due to the lack of a complete endomembrane system.[40] The propelling power, however, is generated in the mitochondria in the sperm's midpiece.[36] As DOX-HCl also interferes with the macromolecular synthesis in mitochondria,[41] it may thus inhibit the energy metabolism of sperms, which is probably the reason for the observed decrease of the sperm's average swimming velocity from 73 ± 16 to 57 ± 17 $\mu$m/s during the loading process (with DOX-HCl solution at 100 $\mu$g/mL), which is, nonetheless, still an acceptable velocity to serve the sperms' purpose. Therefore, also taking into account the observation that the velocity significantly decreased when the DOX-HCl concentration was higher than 100 $\mu$g/mL, we used a concentration of 100 $\mu$g/mL DOX-HCl to load the sperms for the subsequent experiments. Another advantage of sperms comes from their incomplete metabolic system,[40] as a sperm can protect a contained drug within its lipid bilayer like a liposome but does not metabolize it like a stem or other somatic cell would do.

We also carried out a test on the encapsulation stability. The results show that less than 10% of drug was leaked into the medium after 8 h (Figure S4). This means that the DOX-HCl encapsulation by sperm is sufficiently stable for subsequent drug delivery experiments.

**Antitumor Efficacy of Drug-Loaded Sperms.** HeLa cells, as derived from cervical cancer cells, were cultured into spheroids as a 3D tumor model to evaluate the influence of drug-loaded sperms on cell death (see details in the Methods section).[42] In order to visualize the drug distribution into the tumor spheroid, we first employed FITC-BSA as a model for protein-based drugs (Figure S5). We observed that after 24 h co-incubation of BSA-loaded sperms and spheroids, sperms were found not only in the solution but also in the spheroids, as shown in the overlaid z-stack images, demonstrating the tissue penetration capability of sperms. According to a semi-
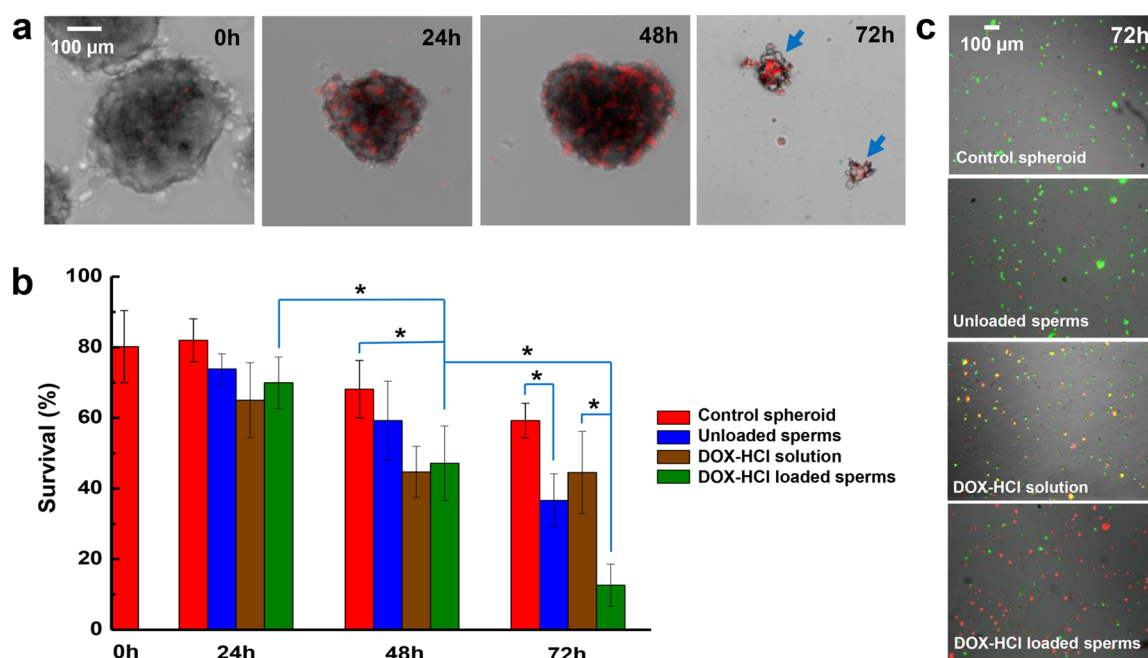
Figure 2. Cell-killing effect of DOX-HCl-loaded sperms on HeLa spheroids. (a) Overlaid *z*-stack images of HeLa spheroids under treatment by DOX-HCl-loaded sperms. Red color shows the fluorescence of DOX-HCl under an excitation light with a wavelength of 470 nm. Blue arrows point at ruptured spheroids. (b) Histogram of the percentage of live cells relative to the total amount of cells at different time points (*n* = 4, cell count = $10^4$ for each sample, *p* < 0.01, ANOVA analysis). (c) LIVE/DEAD staining images of cells from digested spheroids at 72 h.

quantitative analysis using ImageJ, the integrated fluorescence intensity, which represents the total amount of BSA, increased 1.8 times compared to the amount at the beginning of the experiment. The observed spreading area of FITC-BSA increased 7.4 times. This indicates that the increase of the fluorescent area was not only because more sperms swam into the spheroid over time but also because more FITC-BSA was transferred from sperms into the HeLa spheroid. Then, in order to evaluate the antitumor efficacy of drug-loaded sperms, they were loaded with DOX-HCl.

The cell-killing efficacy of DOX-HCl was investigated by co-incubation of DOX-HCl-loaded sperms ($8 \times 10^4$ sperms in 100 $\mu$L of SP-TALP) with HeLa spheroids. Spheroids without any sperms or drug, with unloaded sperms, and with DOX-HCl solution were cultured as control experiments. As mentioned before, $8 \times 10^4$ sperms in 100 $\mu$L solution can be loaded at the maximum of 1.5 $\mu$g of DOX-HCl. Therefore, the control group using DOX-HCl solution was prepared with the same drug concentration (1.5 $\mu$g DOX-HCl in 100 $\mu$L of SP-TALP) for comparison purposes. Figure 2a illustrates the drug transport into a spheroid over 72 h after the treatment with DOX-HCl-loaded sperms. Red fluorescence shows the average intensity of 36 overlaid *z*-stack images, indicating the presence of DOX-HCl. DOX-HCl was found increasingly in the center of the spheroid over time. After 72 h, the size of all spheroids decreased due to the drug-induced cell death. Consequently, broken clusters and ruptured cells were observed in the medium (Figure 2a at 72 h). Cell viability analysis was performed by the LIVE/DEAD test (Figure 2b,c).[43] In the first 24 h of culture, there was no significant change in all groups, while after 48 h, DOX-HCl-loaded sperms showed a cell-killing effect comparable to that of the DOX-HCl solution treatment with the same amount of drug. A lower percentage of live cells was found after the treatment with DOX-HCl-loaded sperms (47%) or DOX-HCl solution (45%) compared to the spheroid

control group (68%). After 72 h, no significant decrease of cell viability was found in the samples of control spheroid and DOX-HCl solution. In contrast, the sample with DOX-HCl-loaded sperms showed the lowest percentage of live cells (13%) among all groups. Unloaded sperms showed a negative effect on HeLa spheroids as well as the percentage of live cells was only 37%, probably attributed to the spheroid disintegration induced by the sperm beating and hyaluronidases reaction. Hyaluronidases are enzymes expressed by sperms to catalyze the degradation of hyaluronic acid, the extracellular matrix of oocyte-surrounding cumulus cells.[44] However, it is also well-known that hyaluronic acid plays an important role in the proliferation and migration of tumor tissue.[45] Therefore, the motility and the hyaluronidases wielded by sperm cells allow them to penetrate deep into a tumor spheroid not only to disintegrate it but also to achieve an effective *in situ* drug administration.

In our experiment, HeLa spheroids were cultured for 3 days before treatment. During cell culture in the lab, HeLa spheroids sustain a balance between cell proliferation and death.[46] As the spheroid grows, the number of both live and dead cells increases. This occurs especially in the necrotic core of the spheroid, as the nutrients from the medium can hardly reach the interior cells. Since DOX-HCl in solution phase can be rapidly taken in by the outer cell layer of spheroids, a pronounced effect of the DOX-HCl solution group in the first 48 h was observed. However, when diluted in the cell medium, DOX-HCl solution was apparently not sufficient to induce the death of more cells from 48 to 72 h (Figure 2b,c). This manifests an advantage of the sperm-hybrid delivery system for the *in vivo* application scenario: the ability to avoid drug dilution in body fluids. By combining the drug encapsulation and tissue penetration capabilities of sperms, and the cell-killing efficacy of the drug, it was possible to achieve a killing efficacy
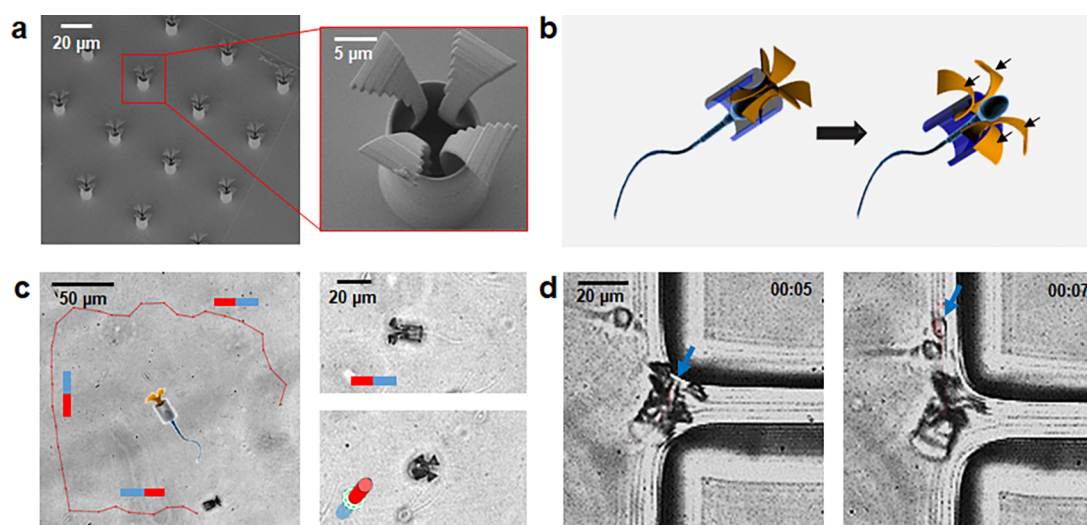
**Figure 3.** (a) SEM images of an array of printed tetrapod microstructures. (b) Schematic illustrating the mechanical release mechanism. (c) Track (red line) of a sperm-hybrid motor under magnetic guidance in the horizontal and vertical planes. (d) Image sequence of a sperm release process when the arms hit the corner of a PDMS wall. Blue arrows point at the sperm head. Time lapse in min:s.

of about 90% after 72 h treatment with DOX-HCl-loaded sperm cells (Figure 2b,c).

**Sperm Transport and Drug Delivery.** In order to demonstrate the potential application of sperms for targeted drug delivery, we fabricated a tetrapod microstructure to guide and release the sperms locally. The tetrapod was designed to have a tubular body and four flexible arched arms. These arms protrude from one opening of the microtube in a curved manner. The dimensions of the microstructure are shown in Figure 3a. At the narrowest point between the four arms, the maximum distance is 4.3 $\mu$m. In preliminary experiments, the dimensions of the structure were optimized according to the dimensions of the sperm cell (for the experiments shown in this paper, bovine sperm cells were selected for their paddle-like shape similar to human sperms), of which the head is, on average, 4.5 $\mu$m wide, 1 $\mu$m thick, and 10 $\mu$m long.[47,48] Therefore, the sperm can be captured to propel the microstructure. Once the arms hit a substantial barrier, such as a cell cluster, they bend and thus enlarge the distance between the arms, allowing the sperm cell to escape from the tube in the process (Figure 3b). The polymeric structure was designed and fabricated by two-photon 3D nanolithography. Then the tetrapod microstructure was asymmetrically coated with 10 nm of iron with a tilt angle of 15° to create a magnetic "easy axis". An additional layer of 2 nm of titanium was deposited to improve the composite's biocompatibility. A finite element simulation was performed to validate the bending capability of the tetrapod geometry. By calculation, when a force of about 128 pN (average sperm force obtained from literature)[49] was applied to one of the arms, the resulting displacement was 116 nm (Figure S6), which was enough to release the sperm. The displacement would increase up to 407 nm when the applied force is 450 pN, which could be generated by a hyperactivated sperm (which exhibits larger tail amplitude and asymmetric beating pattern).[49] Sperm cells were hyper-activated *in vitro* by adding progesterone[50] to the sperm medium as explained in the method section. Video S1 demonstrates the elasticity of the tetrapod arms by repeatedly pressing an arm with an AFM tip toward the substrate. The arms were bent but returned to their original position without damage.

When a sperm reaches a tetrapod, it becomes mechanically trapped inside the cavity of the tubular body and starts to push the tetrapod forward (Video S2). The tubular body of the tetrapod is only 2 $\mu$m longer than the sperm head, thus the sperm tail can still beat freely outside the tube to provide powerful propulsion.[51] Compared to free sperms, the average swimming velocity of the sperm-hybrid motors is decreased by 43% from 73 ± 16 to 41 ± 10 $\mu$m/s (average of 15 samples of sperm-hybrid motors). All measurements were performed in SP-TALP at room temperature. Despite the variability among different sperm samples, the main reason for the velocity reduction is thought to be the increase of the fluid drag that is provoked by the synthetic material and the complex structure of the tetrapod. The asymmetrically distributed metal coating makes possible the guidance of individual sperm-hybrid micromotors using an external magnetic field (Video S3) and even guide a group of them simultaneously (Video S4). Here, more than 50 tetrapods were coupled to sperms within 1 h of incubation, from 648 tetrapods that were counted at the beginning of the experiment. Video S4 shows one of the observation areas, where a group of sperm-hybrid micromotors were guided with an external magnetic field and then how two of them reached the cancer spheroid one next to the other. Figure 3b illustrates a rectangular track of a guided sperm-hybrid motor, also shown in Video S3. The hybrid motor was easily steered by changing the direction of the external magnet. After coupling to a tetrapod, the sperm still rotates when the hybrid motor moves forward due to the helical motion of the sperm,[52] which means the tetrapod does not change the characteristic motion of the coupled sperm. The vertical guidance of a sperm-tetrapod is also shown in Figure 3c. The sperm-hybrid motor was steered to swim vertically out of plane simply by tilting the external magnet vertically. Before starting the experiments with sperm cells, tetrapods were treated with Pluronic F-127 solution to reduce undesired adhesion[53] between the sperm membrane and the tetrapod surface. Video S5a shows the motion of the sperm-tetrapod without adhesion in which the sperm cell rotates inside the tetrapod. In the nonadhesion situation, sperms immediately swam out when the tetrapod arms hit an obstacle. However, the majority of tetrapods were found to rotate together with captured sperms
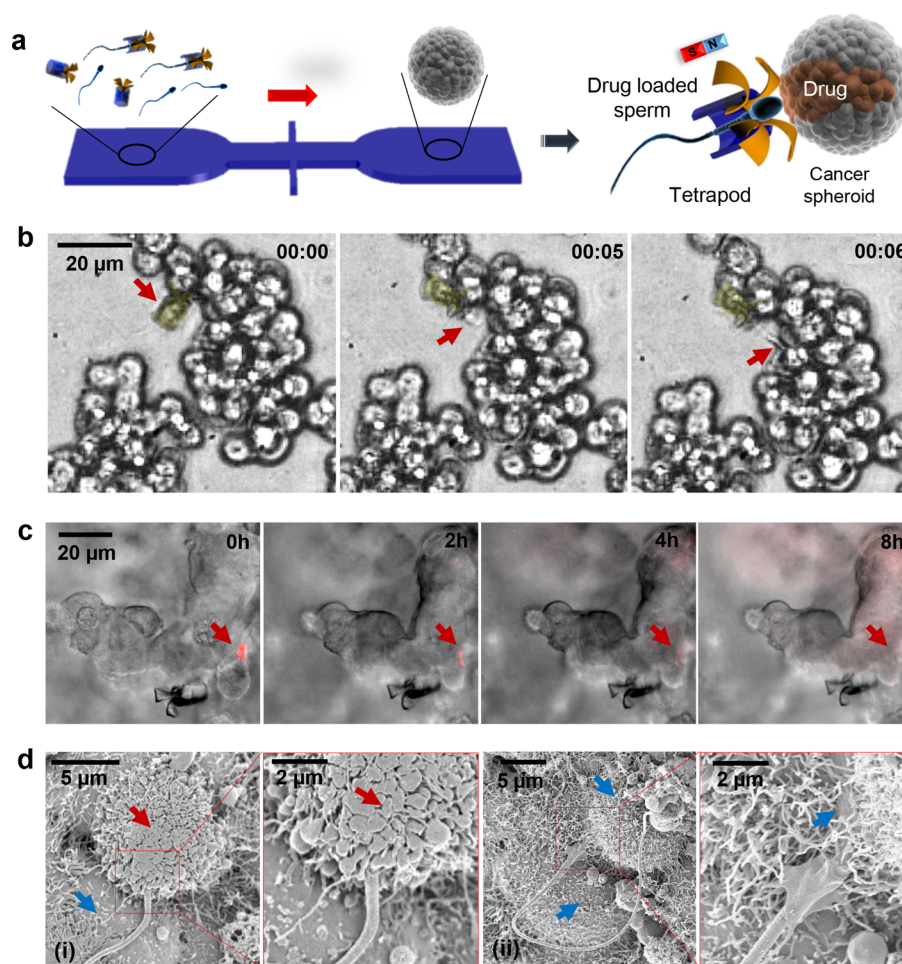
**Figure 4.** (a) Schematic of the microfluidic chip for drug-loaded sperm transport and delivery. (b) Image sequence of the sperm release process when the arms hit HeLa cells. Time lapse in min:s. Red arrows point at the sperm head. (c) DOX-HCl distribution in a HeLa spheroid with overlaid $z$-stack images of the fluorescence channel (20 images with a stack separation distance of 2 $\mu$m). Red arrows point at the sperm head. (d) SEM images showing the sperm−HeLa cell fusion. (i) Cell fusion with the DOX-HCl-loaded sperm; (ii) cell fusion with an unloaded sperm. Red arrows point at a cell in apoptosis and the blue arrows point at live cells.

due to either surface interaction between the sperm membrane and the material surface or the mechanical locking of the sperm head inside the structure (Figure 3c,d). In these cases, it always took several seconds from the moment when the tetrapod hit a wall until complete release of the contained sperm (Video S5b,c), which we found beneficial to release the sperm specifically when the sperm reaches the intended target and hits it for longer time.

Polydimethilsiloxane (PDMS) microfluidic channels were fabricated as a platform for the investigation of the sperm release mechanism. Sperm release occurred in both cases when two arms hit a corner (Video S5a,b) or when four arms hit a wall (Video S5c), while the release processes were different. When the motors came into contact with the targeted barriers, they still rotated for a while after the forward swimming was stopped. The sperm-tetrapod rotation stopped faster when two arms hit a corner because of the geometric gap between the arms which became easily stuck at the corner. Once the rotation stopped, the sperm cell escaped when the tetrapod arms opened (release in around 7 s). When four arms hit a wall, the rotation was not stopped because the arms were not locked. Thus, the sperm release took longer when four arms were bent on a wall (around 12 s). In both cases, tetrapods were pushed back by around 3 $\mu$m after the sperms escaped. The reason for

this recoil is the elasticity of the tetrapod arms which snap back to their original shape once the pushing ceases after the sperm release. Even though there is a substantial diversity in bovine sperm dimensions, swimming behaviors, and fabricated tetrapods within a sample, more than 2/3 (15 out of 22) of the coupled motors were shown to successfully release sperm cells.

The mechanically triggered release performance relies on the elasticity of the tetrapod arms and the sperm force. The calculated deformation of 407 nm that we obtained from simulations is comparable to other similar structures in literature.[54] For example, a microscale beam, which was also fabricated by two-photon lithography, was deflected by around 5 $\mu$m upon a force application of 68 pN.[55] It has also been demonstrated that the type of monomer and the cross-linking parameters contribute to the elasticity of photosensitive polymeric materials.[54] Thus, in order to avoid accidental release events, we did not choose a softer polymer material but optimized the laser power that initialized cross-linking (*ca.* 5 mW) instead. In our simulation, the applied force was given according to the maximum pushing force of a sperm in low-viscosity fluid (2.29 × 10$^{-3}$ Pa·s).[56] In addition, a sperm can generate a more powerful force when the head is pushing against an obstacle, as has been reported previously.[57]

Moreover, the sperm force can be up to 20 times higher when the sperm is hyperactivated and swims in the viscoelastic fluid of the female reproductive system.[49] All these parameters should be considered for future experiments in more realistic environments.[58]

*In vitro* drug delivery experiments were also performed in a microfluidic channel (Figure 4a) to investigate the potential application of the sperm-hybrid micromotors for drug delivery. In order to observe the sperm release in detail, sperm-hybrid micromotors were first guided to HeLa cell clusters by using external magnetic fields (Figure 4b and Video S6). Figure 4b shows an example of how a coupled sperm cell was released on the cell cluster and adhered to one of its cells. The same sperm release mechanism was observed with DOX-HCl-loaded sperm-hybrid micromotors that targeted dense HeLa spheroids. Video S7 shows a sperm that was guided and released on a HeLa cell tumor spheroid, infiltrating it in the process. In this case, the motility of drug-loaded sperms was confirmed before coupling to the tetrapods (Video S8). Video S9 displays the transport of a DOX-HCl-loaded sperm cell through a microfluidic constriction channel and its release into a tumor spheroid. The distance traveled in this experiment was *ca.* 1.8 cm in total, and the journey took approximately 8 min. The sperm cell was released as the tetrapod arms hit the outer boundary of the tumor spheroid and then continued swimming through it until it adhered to one of the cells. Figure 4c shows the release distribution of delivered DOX-HCl over 8 h. The measured fluorescence intensity of the drug-loaded sperm decreased, while the fluorescence signal spread over the spheroid over time. This indicates that DOX-HCl was released from the sperm cell into the spheroid. After 8 h, the targeted HeLa cell experienced a significant cell body shrinkage (size decreased by about 40%), which is known to be a sign of the first stage of cell apoptosis.[55] Figure 4d shows scanning electron microscopy images of the membrane fusion of sperms and HeLa cells. A HeLa spheroid that was treated with unloaded sperms served as a control sample in this experiment. Twenty-four hours after the sperm release event, the anterior part of the sperm head was fused with the targeted HeLa cell, while the midpiece and the flagellum remained outside. Blebs and vesicles were observed on the HeLa cell that fused with a DOX-HCl-loaded sperm, indicating its death by apoptosis (Figure 4d(i)). Cells fused with unloaded sperms did not show such blebs (Figure 4d(ii)) and thus were presumably still alive, just as unfused cells. In literature, this interaction between sperm cells and somatic cells was reported to be attributed to the somatic fusion ability of the spermatozoa during the acrosome reaction.[28] So, by taking advantage of this sperm cell fusion ability, the direct transfer of the drug from sperms to cancer cells minimizes the dilution of drugs into the extracellular matrix or body fluids. At the current stage, the dosage that one single delivered sperm carried, and the resultant drug distribution that could be observed nearby after tumor infiltration, was apparently not sufficient to induce the cell death of the whole spheroid. This makes the investigation of multisperm transport necessary, which will be pursued in future studies to achieve effective tumor treatment.

## CONCLUSIONS

In summary, we have proposed a drug delivery system based on sperm-hybrid micromotors. In such an assembly, sperms are utilized as drug carriers for potential cancer treatment in the female reproductive tract, as the sperm can swim into a tumor spheroid and fuses with somatic cells,[59] transferring the drug

efficiently to the target cell/tumor in the process. Moreover, the sperm cell serves as a propulsion source, while a magnetic microstructure is used for the guidance and release of the sperm: when the arms of the microstructure hit HeLa cells, they bend and thus open a way to free the sperm cell. In this work, bovine sperms were used as model cells to load DOX-HCl drug to treat *in vitro* cultured HeLa cells spheroids. DOX-HCl was locally distributed into the spheroids, showing higher tumor cell-killing efficacy (87%) within the first 72 h, compared to simple drug solution (55%) with the same dose. Sperms also showed a high drug encapsulation capacity of *ca.* 15 pg per sperm. Furthermore, the sperms were able to swim through longer distances under physiological conditions in an efficient manner not only due to their tail beating but also due to their membrane biochemistry. Sperms can remain functional in the human body for a longer time in comparison to other foreign cells due to their ability to inhibit the immune response, by displaying specific proteins[60] and prostasomes[61] on their membrane. This makes this system more compatible to the host body. Compared to purely synthetic micromotors or other carriers, the sperm-hybrid micromotor proposed here can encapsulate high concentrations of drug inside the sperm membrane and hence protect it from the dilution in the body fluids and enzyme degradation. Also, the ability of sperms to fuse with somatic cells represents a unique property to deliver the drug locally into cancer cells through sperm-cell membrane fusion. After drug loading, the activity of the drug and the motility of the sperms are still maintained at a high level due to the sperm cell's incomplete metabolism that eludes intracellular function of the drug. Such sperm-hybrid micromotors not only have potential applicability for gynecologic cancer treatment but also for the therapy of other diseases in the female reproductive tract such as endometriosis or ectopic pregnancies. Moreover, they can be engineered to carry genes, mRNA, imaging contrast agents, or other substances of interest for diverse biomedical applications. Although there are still some challenges to overcome before this system can be applied in *in vivo* environments,[62] such as imaging, biodegradation of the synthetic part, undesired immunoreactions, and controlled doses, sperm-hybrid systems may be envisioned to be applied in *in situ* diagnosis and treatment in the near future.

## METHODS

**Microfluidic Platform Fabrication.** Microfluidic channels were fabricated by soft lithography. Briefly, a silicon wafer was spin-coated with the negative photoresist SU-8 (SÜSS Microtec) and patterned by maskless lithography (μPG 501 Maskless Aligner, Heidelberg Instruments). After that, a mixture of PDMS and curing agent (Dow Corning Corp.) was poured onto the obtained mold and cured at 75 °C for 2 h. The channels were designed to be 200 μm deep and 3 cm long. Two reservoirs were punched out at the inlet and the outlet after peeling off the PDMS channel from the mold. Finally, to complete the channel fabrication, the PDMS channel and a cleaned glass substrate were physically bonded after being exposed to oxygen plasma for about 30 s. To treat the inner channel surface, channels were filled with Pluronic F-127 solution (10 μg/mL in DI water) (Sigma-Aldrich, Germany) and incubated for 1 h at 37 °C. Pluronic F-127 has been previously used to repel sperm cells, making it suitable for minimizing unspecific adhesion between sperms, the channel, and synthetic component surfaces.[53] After this treatment, the channels were rinsed with water and sperm medium (SP-TALP, see Table S1) three times before starting the experiment.

**Tetrapod Fabrication.** Arrays of polymeric tetrapods were fabricated by 3D laser lithography (Photonic Professional GT, Nanoscribe GmbH). Briefly, dip-in laser lithography photoresist (IP-

Dip, Nanoscribe GmbH) was drop-cast onto cleaned quartz glass substrates ($25 \times 25$ mm$^2$) as the basis polymer material for laser writing. The negative-tone photoresist was then polymerized specifically at preprogrammed exposure positions by two-photon absorption (laser wavelength 780 nm). The design of the tetrapod arrays was programmed with DeScribe software (Nanoscribe GmbH). The samples were then dried in a critical point dryer (CPD, Autosamdri-931, Tousimis Research Corporation) after 20 min of development in mr-Dev 600 (Micro Resist Technology GmbH) and 3 min of washing in isopropyl alcohol. The dried samples were coated with 10 nm Fe and 2 nm Ti of high purity (99.995%) by e-beam metal evaporation (Edwards auto 500 e-beam, Moorfield Nanotechnology Limited). To create a magnetic easy axis, the sample holder was tilted at an angle of 75° during the deposition process. The metal-coated samples were also immersed in Pluronic F-127 solution for 1 h at 37 °C and rinsed with water and SP-TALP for subsequent experiments to avoid unspecific adhesion of target cells.

Tetrapod printing quality was evaluated by scanning electron microscopy (Zeiss NVision 40, Carl Zeiss Microscopy GmbH). The samples were fixed on a metal stub and coated with 10 nm of platinum. Imaging was performed at a working distance of 5 mm in the secondary electron imaging mode at a working voltage of 2 kV.

The finite element analysis of the arm deformation was performed with Autodesk Inventor software (applied Young's modulus and Poisson ratio are 0.15 GPa and 0.45, respectively).[63] The relationship between the deflection and the distributed load was calculated according to the Euler−Bernoulli equation[64] as

$$q = \frac{d^2}{dx^2}\left(EI\frac{d^2\omega}{dx^2}\right)$$

where $\omega$ and $q$ represent the deflection and distributed load, respectively, $x$ describes the orientation direction of an arm, $E$ is the Young's modulus of the material, and $I$ is the second moment of area of an arm's cross section. For an arm with a loading along the $z$ axis

$$I = \iint z^2 \mathrm{d}y\mathrm{d}z$$

**Culture of HeLa Cell Spheroids.** HeLa cells were cultured in a 25 mL adherent flask for 2 weeks after recovering (for details of the medium, see Table S2). To prepare tumor spheroids, the cells were first incubated in 2 mL of trypsin/EDTA for 10 min to be detached from the substrate. After dilution in 8 mL of medium, the cell suspension was then centrifuged at 1000 rpm for 3.5 min to remove the medium. Then the cell pellet was resuspended in 1 mL of medium. After calculation, $3 \times 10^5$ cells were suspended into 3 mL of medium and seeded in a spheroid culture dish (Cellstar Cell-Repellent Surface, Greiner bio-one).[65] After 3 days maturation, the spheroid solution was transferred into a 15 mL falcon and incubated for 5 min to separate the sediment cells. Finally, the bottom pellet of the spheroids was resuspended in 3 mL of new medium in the spheroid culture dish for subsequent experiments.

**Preparation of Drug-Loaded Sperm Cells.** Bovine sperm cells were recovered by thawing cryopreserved sperm straws rapidly in a water bath at 38 °C for 2 min and washed with BoviPure 100/BoviDilute (40%/80%).[66] After 5 min centrifugation at 300$g$ in soft mode, the sperms were resuspended in 1 mL of SP-TALP for subsequent use. Sperm concentration was calculated by using a cell counting chamber. One mg/mL of FITC-BSA (Sigma-Aldrich, Germany) and DOX-HCl (Sigma-Aldrich, Germany) solution was prepared in SP-TALP and stored under dark conditions at 4 °C as stock solutions. To prepare DOX/BSA-loaded sperm cells, a mixture of sperm solution and FITC-BSA or DOX-HCl solution at specific concentrations were co-incubated in a humidified atmosphere of 5% CO$_2$ in air at 37 °C for 1 h. After the sample was washed two times with SP-TALP by centrifugation at 300$g$ for 5 min, the pellet of drug-loaded sperms was redispersed in SP-TALP with progesterone (20 ng/mL) and stored in the incubator under dark conditions for subsequent use. It is important to note that the samples were to be used within 4 h to guarantee sperm motility.

**Evaluation of the Drug Loading Efficiency.** The success of the drug loading procedure was evaluated by the determination of the encapsulation efficiency. DOX-HCl-loaded sperm cells were prepared as mentioned before with a concentration of $3 \times 10^6$ sperms/mL. The samples of DOX-HCl solution were designed as a series of concentrations with 10, 20, 50, 100, and 200 $\mu$g/mL. FITC-BSA-loaded sperms were prepared with FITC-BSA solution with a concentration of 100 $\mu$g/mL. After incubation of sperms in these solutions, the respective supernatant was collected after centrifugation and filtered through a 2 $\mu$m pore size membrane. The sperms were resuspended after purification as mentioned before. Fluorescence images were taken at an excitation wavelength of 470 nm (DOX-HCl: ex 470 nm, em 580 nm;[67] FITC-BSA: ex 470 nm, em 509 nm[68]) (Cell Observer, Carl Zeiss Microscopy GmbH). The concentration of DOX-HCl was determined with a fluorescence spectrometer in FL-RL mode (SpectraMax M2, Molecular Devices, LLC), and the total weight was calculated. SP-TALP solution was used as blank control for all measurements. The concentration of the residual DOX-HCl was determined by measuring the supernatant of each sample after centrifugation. The encapsulation efficiency was calculated as the ratio of encapsulated drug to the total amount of the used drug:

$$\begin{aligned} &\text{DOX loading ratio} \\ &= \frac{\text{total weight of used DOX} - \text{weight of residual DOX}}{\text{total weight of used drug}} \end{aligned}$$

$$\text{DOX amount per sperm} = \frac{\text{total loading amount}}{\text{number of used sperms}}$$

The drug loading amount was determined by the difference between the initial amount of DOX-HCl before incubation and the residual amount in the supernatant after co-incubation, which were both quantified by their respective fluorescence signals.

The encapsulation stability test was carried out by calculating the accumulative release ratio of DOX-HCl from sperms into SP-TALP. Briefly, drug-loaded sperms were incubated in SP-TALP in a dark place under humidified atmosphere, 5% CO$_2$ and 37 °C. At each time point, the samples were centrifuged and 0.5 mL of supernatant was collected and replaced with 0.5 mL of SP-TALP. After 96 h, the samples were treated with EDTA-trypsin for 3 min to release all drug into the solution. A fluorescence spectrometer in FL-RL mode (SpectraMax M2, Molecular Devices, LLC) was used to quantify the DOX-HCl concentration of the supernatant. The accumulative release ratio was calculated as the ratio of the accumulated amount of the drug to the total amount of it. Data were obtained from four samples. SP-TALP was used as blank control.

**Evaluation of DOX-HCl-Loaded Sperm Viability.** DOX-HCl-loaded sperms were prepared as mentioned before by incubating sperms ($8 \times 10^5$ sperms in 1 mL) with DOX-HCl at a concentration of 100 $\mu$g/mL. After purification, sperms were incubated in a humidified atmosphere of 5% CO$_2$ in air at 37 °C. After 1 and 4 h, drug-loaded sperms were analyzed by fluorescence microscopy (Cell Observer, Carl Zeiss Microscopy GmbH), using a commercial LIVE/DEAD viability kit (ThermoFisher). Briefly, sperm solutions ($10^6$ sperms) were incubated with 5 $\mu$L of diluted component A (SYBR 14, 10%) for 10 min and 5 $\mu$L of component B (propidium iodide) for 5 min. After being washed, sperm analysis was performed at an excitation wavelength of 470 nm to visualize the live sperms. Four samples for each group with $10^4$ sperms per sample were used for the analysis.

**Evaluation of the Motility of DOX-HCl-Loaded Sperms.** DOX-HCl-loaded sperms were prepared as mentioned before. Unloaded sperms were treated with the same method as the control sample. After purification, sperms were incubated in SP-TALP in a humidified atmosphere of 5% CO$_2$ in air at 37 °C. At certain time points along 36 h, 100 $\mu$L of sperms ($10^4$ per each sample) was extracted from the Petri dish and added into the counting chamber to study the motility. For that, a computer-assisted sperm analysis system (AndroVision, Minitube GmbH) was employed. Four samples were

prepared for each group. Ten fields (*ca.* 500 sperms) of each sample were counted at each time point.

**Evaluation of Antitumor Efficacy of DOX-HCl-Loaded Sperms.** DOX-HCl-loaded sperms were prepared as mentioned before by incubating blank sperms ($8 \times 10^5$ sperms in 1 mL) with DOX-HCl at a concentration of 100 $\mu$g/mL. After purification, 100 $\mu$L of sperm solution ($8 \times 10^4$ sperms) was added into a HeLa spheroid suspension (4 mL) and co-incubated in a humidified atmosphere of 5% $CO_2$ in air at 37 °C. Spheroid control was prepared by adding 100 $\mu$L of SP-TALP, while blank sperm control was prepared by adding 100 $\mu$L of blank sperm solution ($8 \times 10^4$ sperms). According to the loading ratio of DOX-HCl (15%), at the maximum 15 $\mu$g of DOX-HCl (100 $\mu$L) can be loaded into sperms in 1 mL of solution. Therefore, DOX-HCl solution control was prepared by incubating HeLa spheroids with 100 $\mu$L of DOX-HCl solution at a concentration of 15 $\mu$g/mL. The LIVE/DEAD viability kit (ThermoFisher) was employed to stain cells and analyze the cell viability. Briefly, HeLa spheroids were washed and digested by trypsin-EDTA to a single-cell suspension at certain time points. After that, cells were incubated with 1 $\mu$L of component A (SYBR 14) for 10 min and 5 $\mu$L of component B (propidium iodide) for 5 min. Cell counting was performed under excitation at the wavelength of 470 nm for live cells and 540 nm for dead cells (4 samples for each group, $10^4$ cells for each sample) (Cell Observer, Carl Zeiss Microscopy GmbH).

**Evaluation of Sperm Transport Procedure.** PDMS-based microfluidic chips were employed to evaluate the sperm-tetrapod coupling procedure, the magnetic guidance of sperm-hybrid motors, and the sperm release by the mechanical trigger function. The chip featured a 500 $\mu$m wide channel where the sperm-tetrapod coupling and guidance occurred and obstacles in three different shapes where the sperm release occurred (see Video S5). Tetrapods, PDMS channels, and sperms were prepared and treated as mentioned before. After that, an array of tetrapods (1296 devices in total) was detached from the substrate by mechanical scratching and dispersed into 50 $\mu$L of SP-TALP. For the evaluation of the sperm-hybrid motor performance, 50 $\mu$L of a mixture of equal parts sperm solution ($3 \times 10^5$ per mL) and tetrapod suspension (*ca.* 750 in 25 $\mu$L of SP-TALP) was introduced into the channel. Real-time videos of the samples were recorded under the microscope (ZEISS Axio Scope. A1, Carl Zeiss Microscopy GmbH) with a high-speed camera (Phantom Miro eX4, Vision Research Inc.) with 30 frames per second. Working temperature was maintained at 38 °C to maintain the motility of the respective sperm sample. After coupling, the sperm-hybrid motor was guided by simply rotating a permanent magnet, and the resulting directional changes were recorded to evaluate the guidance performance. The operating distance between the magnet and the sample was about 10 cm, resulting in an effective magnetic field of roughly 5 mT. Sperm release was evaluated by guiding the coupled motor onto different obstacles.

**Evaluation of Drug-Loaded Sperm Delivery toward Tumor Spheroids.** Figure 4a shows the microfluidic chip that was designed for drug delivery experiments. The chip was designed to have a wide dosing region (where sperms couple to the tetrapods), a treatment region (where the tumor spheroid is located), and a constricted neck region in the middle to prevent the entry of noncoupled sperm cells into the treatment region. Drug-loaded sperms were prepared as mentioned earlier and observed under a fluorescence microscope using an excitation light with a wavelength of 470 nm (see Video S7, exposure time: 500 ms). After chip treatment with Pluronic F-127 and SP-TALP, HeLa cell medium was first filled into the chip as the experimental environment. Then the HeLa spheroid was introduced into the chip from the left end, and then 5 $\mu$L of tetrapod suspension (around 300 tetrapods) and 5 $\mu$L of drug-loaded sperms solution ($3 \times 10^5$ /mL) were introduced from the right end. Real-time videos of the transport process were recorded under the aforementioned microscope at 30 frames/s. With the guidance by an external magnet at a distance of *ca.* 10 cm, sperm-hybrid motors were guided to the target spheroid, and the coupled drug-loaded sperms were released into the spheroid. Afterward, the whole system was incubated in appropriate cell culture conditions (5% $CO_2$ in air at 37 °C). At fixed time points,

*z*-stack images of the sperm embedded spheroids were captured under the aforementioned fluorescence microscope. The exposure time of the fluorescent channel for all images was fixed at 800 ms. Subsequent semiquantitative analysis of the multichannel images was executed with ImageJ.

**SEM Characterization of Sperm−HeLa Cell Fusion.** SEM samples were prepared at 24 h after the sperms swam into the spheroids. The spheroids were transferred onto coverslips and fixed in 2.5% glutaraldehyde in PBS for 8 h. After that, the fixed samples were washed with PBS and dehydrated in an ascending series of isopropyl alcohol solutions and dried in CPD. Then the samples were coated with 20 nm of Pt and examined in a scanning electron microscope (DSM-960, Zeiss).

## ASSOCIATED CONTENT

**Ⓢ Supporting Information**

The Supporting Information is available free of charge on the ACS Publications website at DOI: 10.1021/acsnano.7b06398.

Table S1 and Figures S1−S6 (PDF)
Video S1: Tetrapod arm bending (AVI)
Video S2: Sperm coupling (AVI)
Video S3: Magnetic alignment and guidance (AVI)
Video S4: Guidance of multiple micromotors (AVI)
Video S5: Sperm release on PDMS walls (AVI)
Video S6: Sperm release in a HeLa cluster (AVI)
Video S7: Sperm release in a HeLa spheroid (AVI)
Video S8: Fluorescence of motile DOX-HCl-loaded sperms (AVI)
Video S9: DOX-HCl-loaded sperm release in a HeLa spheroid (AVI)

## AUTHOR INFORMATION

**Corresponding Author**
*E-mail: m.medina.sanchez@ifw-dresden.de.

**ORCID** ⓘ
Mariana Medina-Sánchez: 0000-0001-6149-3732

**Author Contributions**
H.X., M.M.-S., and O.G.S. conceived the project. H.X. and M.M.-S. designed the experiments with help from V.M. and F.H. H.X. performed the experiments with the help of F.H. H.X., M.M.-S., V.M., and O.G.S. analyzed and interpreted the results. H.X. and M.M.-S. wrote the manuscript. L.S. helped with the fabrication. M.M.-S. made the schematic figures. All authors commented and edited the manuscript and figures.

**Notes**
The authors declare no competing financial interest.

## REFERENCES

(1) Cho, K.; Wang, X.; Nie, S.; Chen, Z. G.; Shin, D. M. Therapeutic Nanoparticles for Drug Delivery in Cancer. *Clin. Cancer Res.* **2008**, *14*, 1310−1316.

(2) De Jong, W. H.; Borm, P. J. A. Drug Delivery and Nanoparticles: Applications and Hazards. *Int. J. Nanomed.* **2008**, *3*, 133−149.

(3) Allen, T. M.; Cullis, P. R. Liposomal Drug Delivery Systems: From Concept to Clinical Applications. *Adv. Drug Delivery Rev.* **2013**, *65*, 36−48.

(4) Tannock, I. F.; Lee, C. M.; Tunggal, J. K.; Cowan, D. S.; Egorin, M. J. Limited Penetration of Anticancer Drugs through Tumor Tissue: A Potential Cause of Resistance of Solid Tumors to Chemotherapy. *Clin. Cancer Res.* **2002**, *8*, 878−884.

(5) Allen, T. M.; Hansen, C. B.; de Menezes, D. E. L. Pharmacokinetics of Long-Circulating Liposomes. *Adv. Drug Delivery Rev.* **1995**, *16*, 267−284.

(6) Tan, S.; Wu, T.; Zhang, D.; Zhang, Z. Cell or Cell Membrane-Based Drug Delivery Systems. *Theranostics* **2015**, *5*, 863−881.

(7) Stuckey, D. W.; Shah, K. Stem Cell-Based Therapies for Cancer Treatment: Separating Hope from Hype. *Nat. Rev. Cancer* **2014**, *14*, 683−691.

(8) Xuan, M.; Shao, J.; Dai, L.; Li, J.; He, Q. Macrophage Cell Membrane Camouflaged Au Nanoshells for *In Vivo* Prolonged Circulation Life and Enhanced Cancer Photothermal Therapy. *ACS Appl. Mater. Interfaces* **2016**, *8*, 9610−9618.

(9) Hamidi, M.; Zarrin, A.; Foroozesh, M.; Mohammadi-Samani, S. Applications of Carrier Erythrocytes in Delivery of Biopharmaceuticals. *J. Controlled Release* **2007**, *118*, 145−160.

(10) Magdanz, V.; Sanchez, S.; Schmidt, O. G. Development of a Sperm-Flagella Driven Micro-Bio-Robot. *Adv. Mater.* **2013**, *25*, 6581−6588.

(11) Tanaka, Y.; Morishima, K.; Shimizu, T.; Kikuchi, A.; Yamato, M.; Okano, T.; Kitamori, T. An Actuated Pump on-Chip Powered by Cultured Cardiomyocytes. *Lab Chip* **2006**, *6*, 362−368.

(12) Felfoul, O.; Mohammadi, M.; Taherkhani, S.; De Lanauze, D.; Xu, Y. Z.; Loghin, D.; Essa, S.; Jancik, S.; Houle, D.; Lafleur, M.; et al. Magneto-Aerotactic Bacteria Deliver Drug-Containing Nanoliposomes to Tumour Hypoxic Regions. *Nat. Nanotechnol.* **2016**, *11*, 941−947.

(13) Zhuang, J.; Sitti, M. Chemotaxis of Bio-Hybrid Multiple Bacteria-Driven Microswimmers. *Sci. Rep.* **2016**, *6*, 32135.

(14) Akin, D.; Sturgis, J.; Ragheb, K.; Sherman, D.; Burkholder, K.; Robinson, J. P.; Bhunia, A. K.; Mohammed, S.; Bashir, R. Bacteria-Mediated Delivery of Nanoparticles and Cargo into Cells. *Nat. Nanotechnol.* **2007**, *2*, 441−449.

(15) Stanton, M. M.; Simmchen, J.; Ma, X.; Miguel-López, A.; Sánchez, S. Biohybrid Janus Motors Driven by Escherichia Coli. *Adv. Mater. Interfaces* **2016**, *3*, 1500505.

(16) Stanton, M. M.; Park, B.-W.; Miguel-López, A.; Ma, X.; Sitti, M.; Sánchez, S. Biohybrid Microtube Swimmers Driven by Single Captured Bacteria. *Small* **2017**, *13*, 1603679.

(17) Palffy, R.; Gardlik, R.; Hodosy, J.; Behuliak, M.; Resko, P.; Radvansky, J.; Celec, P. Bacteria in Gene Therapy: Bactofection *Versus* Alternative Gene Therapy. *Gene Ther.* **2006**, *13*, 101−105.

(18) Kiyomiya, K.; Matsuo, S.; Kurebe, M. Proteasome Is a Carrier to Translocate Doxorubicin from Cytoplasm into Nucleus. *Life Sci.* **1998**, *62*, 1853−1860.

(19) Johnson, G. D.; Lalancette, C.; Linnemann, A. K.; Leduc, F.; Boissonneault, G.; Krawetz, S. A. The Sperm Nucleus: Chromatin, Rna, and the Nuclear Matrix. *Reproduction* **2011**, *141*, 21−36.

(20) Kwon, G. S.; Okano, T. Polymeric Micelles as New Drug Carriers. *Adv. Drug Delivery Rev.* **1996**, *21*, 107−116.

(21) Qiu, F.; Fujita, S.; Mhanna, R.; Zhang, L.; Simona, B. R.; Nelson, B. J. Gene Therapy: Magnetic Helical Microswimmers Functionalized with Lipoplexes for Targeted Gene Delivery. *Adv. Funct. Mater.* **2015**, *25*, 1764−1764.

(22) Mhanna, R.; Qiu, F.; Zhang, L.; Ding, Y.; Sugihara, K.; Zenobi-Wong, M.; Nelson, B. J. Artificial Bacterial Flagella for Remote-Controlled Targeted Single-Cell Drug Delivery. *Small* **2014**, *10*, 1953−1957.

(23) de Ávila, B. E. F.; Angsantikul, P.; Li, J.; Lopez-Ramirez, M. A.; Ramírez-Herrera, D. E.; Thamphiwatana, S.; Chen, C.; Delezuk, J.; Samakapiruk, R.; Ramez, V.; et al. Micromotor-enabled Active Drug Delivery for *In Vivo* Treatment of Stomach Infection. *Nat. Commun.* **2017**, *8*, 272.

(24) Srivastava, S. K.; Medina-Sánchez, M.; Koch, B.; Schmidt, O. G. Medibots: Dual-Action Biogenic Microdaggers for Single-Cell Surgery and Drug Release. *Adv. Mater.* **2016**, *28*, 832−837.

(25) Lin, X.; Wu, Z.; Wu, Y.; Xuan, M.; He, Q. Self-Propelled Micro-/Nanomotors Based on Controlled Assembled Architectures. *Adv. Mater.* **2016**, *28*, 1060−1072.

(26) Wu, Z.; Lin, X.; Wu, Y.; Si, T.; Sun, J.; He, Q. Near-Infrared Light-Triggered "On/Off" Motion of Polymer Multilayer Rockets. *ACS Nano* **2014**, *8*, 6097−6105.

(27) Bysell, H.; Månsson, R.; Hansson, P.; Malmsten, M. Microgels and Microcapsules in Peptide and Protein Drug Delivery. *Adv. Drug Delivery Rev.* **2011**, *63*, 1172−1185.

(28) Mattioli, M.; Gloria, A.; Mauro, A.; Gioia, L.; Barboni, B. Fusion as the Result of Sperm-Somatic Cell Interaction. *Reproduction* **2009**, *138*, 679−687.

(29) Makhluf, S. B.-D.; Abu-Mukh, R.; Rubinstein, S.; Breitbart, H.; Gedanken, A. Modified PVA−Fe₃O₄ Nanoparticles as Protein Carriers into Sperm Cells. *Small* **2008**, *4*, 1453−1458.

(30) Geerts, N.; McGrath, J.; Stronk, J.; Vanderlick, T.; Huszar, G. Spermatozoa as a Transport System of Large Unilamellar Lipid Vesicles into the Oocyte. *Reprod. BioMed. Online* **2014**, *28*, 451−461.

(31) Medina-Sánchez, M.; Schwarz, L.; Meyer, A. K.; Hebenstreit, F.; Schmidt, O. G. Cellular Cargo Delivery: Toward Assisted Fertilization by Sperm-Carrying Micromotors. *Nano Lett.* **2016**, *16*, 555−561.

(32) Schwarz, L.; Medina-Sánchez, M.; Schmidt, O. G. Hybrid BioMicromotors. *Appl. Phys. Rev.* **2017**, *4*, 031301.

(33) Tacar, O.; Sriamornsak, P.; Dass, C. R. Doxorubicin: An Update on Anticancer Molecular Action, Toxicity and Novel Drug Delivery Systems. *J. Pharm. Pharmacol.* **2013**, *65*, 157−170.

(34) Ishida, T.; Atobe, K.; Wang, X.; Kiwada, H. Accelerated Blood Clearance of Pegylated Liposomes upon Repeated Injections: Effect of Doxorubicin-Encapsulation and High-Dose First Injection. *J. Controlled Release* **2006**, *115*, 251−258.

(35) Kiyomiya, K.; Matsuo, S.; Kurebe, M. Mechanism of Specific Nuclear Transport of Adriamycin: the Mode of Nuclear Translocation of Adriamycin-Proteasome Complex. *Cancer Res.* **2001**, *61*, 2467−2471.

(36) Rengan, A. K.; Agarwal, A.; van der Linde, M.; du Plessis, S. S. An Investigation of Excess Residual Cytoplasm in Human Spermatozoa and Its Distinction from the Cytoplasmic Droplet. *Reprod. Biol. Endocrinol.* **2012**, *10*, 92.

(37) Munerati, M.; Cortesi, R.; Ferrari, D.; Di Virgilio, F.; Nastruzzi, C. Macrophages Loaded with Doxorubicin by ATP-Mediated Permeabilization: Potential Carriers for Antitumor Therapy. *Biochim. Biophys. Acta, Mol. Cell Res.* **1994**, *1224*, 269−276.

(38) Gill, D. R.; Hyde, S. C.; Higgins, C. F.; Valverde, M. A.; Mintenig, G. M.; Sepúlveda, F. V. Separation of Drug Transport and Chloride Channel Functions of the Human Multidrug Resistance P-Glycoprotein. *Cell* **1992**, *71*, 23−32.

(39) Batrakova, E. V.; Li, S.; Brynskikh, A. M.; Sharma, A. K.; Li, Y.; Boska, M.; Gong, N.; Mosley, R. L.; Alakhov, V. Y.; Gendelman, H. E. Effects of Pluronic and Doxorubicin on Drug Uptake, Cellular Metabolism, Apoptosis and Tumor Inhibition in Animal Models of MDR Cancers. *J. Controlled Release* **2010**, *143*, 290−301.

(40) Gur, Y.; Breitbart, H. Protein Synthesis in Sperm: Dialog between Mitochondria and Cytoplasm. *Mol. Cell. Endocrinol.* **2008**, *282*, 45−55.

(41) Qu, Q.; Ma, X.; Zhao, Y. Targeted Delivery of Doxorubicin to Mitochondria Using Mesoporous Silica Nanoparticle Nanocarriers. *Nanoscale* **2015**, *7*, 16677−16686.

(42) Yuan, F. Stress Is Good and Bad for Tumors. *Nat. Biotechnol.* **1997**, *15*, 722−723.

(43) Ma, H. L.; Jiang, Q.; Han, S.; Wu, Y.; Cui Tomshine, J.; Wang, D.; Gan, Y.; Zou, G.; Liang, X. J. Multicellular Tumor Spheroids as an *In Vivo*-Like Tumor Model for Three-Dimensional Imaging of Chemotherapeutic and Nano Material Cellular Penetration. *Mol. Imaging* **2012**, *11*, 487−498.

(44) Gwatkin, R.; Andersen, O. Effect of Glycosidase Inhibitors on the Capacitation of Hamster Spermatozoa by Cumulus Cells *In Vitro*. *Reproduction* **1973**, *35*, 565−567.

(45) Liu, N.; Gao, F.; Han, Z.; Xu, X.; Underhill, C. B.; Zhang, L. Hyaluronan Synthase 3 Overexpression Promotes the Growth of TSU Prostate Cancer Cells. *Cancer Res.* **2001**, *61*, 5207−5214.

(46) Grimes, D. R.; Kelly, C.; Bloch, K.; Partridge, M. A Method for Estimating the Oxygen Consumption Rate in Multicellular Tumour Spheroids. *J. R. Soc., Interface* **2014**, *11*, 20131124.

(47) Gravance, C. G.; Vishwanath, R.; Pitt, C.; Garner, D. L.; Casey, P. J. Effects of Cryopreservation on Bull Sperm Head Morphometry. *J. Androl.* **1998**, *19*, 704−709.

(48) Van Dilla, M. A.; Gledhill, B. L.; Lake, S.; Dean, P. N.; Gray, J. W.; Kachel, V.; Barlogie, B.; Gohde, W. Measurement of Mammalian Sperm Deoxyribonucleic Acid by Flow Cytometry. Problems and Approaches. *J. Histochem. Cytochem.* **1977**, *25*, 763−773.

(49) Ishimoto, K.; Gaffney, E. A. Mechanical Tuning of Mammalian Sperm Behaviour by Hyperactivation, Rheology and Substrate Adhesion: A Numerical Exploration. *J. R. Soc., Interface* **2016**, *13*, 20160633.

(50) Uhler, M. L.; Leungt, A.; Chan, S. Y.; Wang, C. Direct Effects of Progesterone and Antiprogesterone on Human Sperm Hyperactivated Motility and Acrosome Reaction. *Fertil. Steril.* **1992**, *58*, 1191−1198.

(51) Magdanz, V.; Medina-Sánchez, M.; Chen, Y.; Guix, M.; Schmidt, O. G. How to Improve Spermbot Performance. *Adv. Funct. Mater.* **2015**, *25*, 2763−2770.

(52) Jikeli, J. F.; Alvarez, L.; Friedrich, B. M.; Wilson, L. G.; Pascal, R.; Colin, R.; Pichlo, M.; Rennhack, A.; Brenker, C.; Kaupp, U. B. Sperm Navigation Along Helical Paths in 3D Chemoattractant Landscapes. *Nat. Commun.* **2015**, *6*, 7985.

(53) Frimat, J. P.; Bronkhorst, M.; de Wagenaar, B.; Bomer, J. G.; van der Heijden, F.; van den Berg, A.; Segerink, L. I. Make It Spin: Individual Trapping of Sperm for Analysis and Recovery Using Micro-Contact Printing. *Lab Chip* **2014**, *14*, 2635−2641.

(54) Sun, H.-B.; Kawata, S. Two-Photon Photopolymerization and 3d Lithographic Microfabrication. *Adv. Polym. Sci.* **2006**, *170*, 169−274.

(55) Ha, C. W.; Yang, D.-Y. Rotational Elastic Micro Joint Based on Helix-Augmented Cross-Spring Design for Large Angular Movement. *Opt. Express* **2014**, *22*, 20789−20797.

(56) Ishijima, S. Dynamics of Flagellar Force Generated by a Hyperactivated Spermatozoon. *Reproduction* **2011**, *142*, 409−415.

(57) Nosrati, R.; Graham, P. J.; Liu, Q.; Sinton, D. Predominance of Sperm Motion in Corners. *Sci. Rep.* **2016**, *6*, 26669.

(58) Friis, M. B.; Friborg, C. R.; Schneider, L.; Lambert, I. H.; Christensen, S. T.; Hoffmann, E. K. Cell Shrinkage as a Signal to Apoptosis in NIH 3T3 Fibroblasts. *J. Physiol.* **2005**, *567*, 427−443.

(59) Bendich, A.; Borenfreund, E.; Sternberg, S. S. Penetration of Somatic Mammalian Cells by Sperm. *Science* **1974**, *183*, 857−859.

(60) Rooney, I. A.; Oglesby, T. J.; Atkinson, J. P. Complement in Human Reproduction: Activation and Control. *Immunol. Res.* **1993**, *12*, 276−294.

(61) Kelly, R. W.; Holland, P.; Skibinski, G.; Harrison, C.; McMillan, L.; Hargreave, T.; James, K. Extracellular Organelles (Prostasomes) Are Immunosuppressive Components of Human Semen. *Clin. Exp. Immunol.* **1991**, *86*, 550−556.

(62) Medina-Sánchez, M.; Schmidt, O. G. Medical Microbots Need Better Imaging and Control. *Nature* **2017**, *545*, 406−408.

(63) Bückmann, T.; Kadic, M.; Schittny, R.; Wegener, M. Mechanical Metamaterials with Anisotropic and Negative Effective Mass-Density Tensor Made from One Constituent Material. *Phys. Status Solidi B* **2015**, *252*, 1671−1674.

(64) Park, S.; Gao, X. Bernoulli−Euler Beam Model Based on a Modified Couple Stress Theory. *J. Micromech. Microeng.* **2006**, *16*, 2355−2359.

(65) Froehlich, K.; Haeger, J.-D.; Heger, J.; Pastuschek, J.; Photini, S. M.; Yan, Y.; Lupp, A.; Pfarrer, C.; Mrowka, R.; Schleußner, E.; et al. Generation of Multicellular Breast Cancer Tumor Spheroids: Comparison of Different Protocols. *Journal of Mammary Gland Biology and Neoplasia.* **2016**, *21*, 89−98.

(66) Samardzija, M.; Karadjole, M.; Getz, I.; Makek, Z.; Cergolj, M.; Dobranic, T. Effects of Bovine Spermatozoa Preparation on Embryonic Development *In Vitro*. *Reprod. Biol. Endocrinol.* **2006**, *4*, 58.

(67) Kumar, R.; Kulkarni, A.; Nagesha, D. K.; Sridhar, S. *In Vitro* Evaluation of Theranostic Polymeric Micelles for Imaging and Drug Delivery in Cancer. *Theranostics* **2012**, *2*, 714−722.

(68) Chudakov, D. M.; Verkhusha, V. V.; Staroverov, D. B.; Souslova, E. A.; Lukyanov, S.; Lukyanov, K. A. Photoswitchable Cyan Fluorescent Protein for Protein Tracking. *Nat. Biotechnol.* **2004**, *22*, 1435−1439.